

Orbits of Binary Stars: from Visual Measures to Speckle Interferometry

ANDREI TOKOVININ¹

¹*Cerro Tololo Inter-American Observatory — NFSs NOIRLab Casilla 603, La Serena, Chile*

ABSTRACT

Knowledge of the orbits of visual binary stars has always been one of the fundamentals of astronomy. Based historically on the visual measures, nowadays the orbits rely more (or exclusively) on the accurate speckle data. This prompts reconsideration of the methods of orbit calculation, undertaken here and illustrated by 20 examples, from accurate to drastically revised and tentative orbits. Good understanding and critical assessment of the input data is a key requirement, especially concerning visual measures. Combination of visual and speckle data is still needed for long-period binaries, but the relative weights must match their respective errors. When the orbit can be fully constrained only by accurate speckle data, the old measures should be ignored. Orbits can be classified into three grades: A — fully constrained, B — semi-constrained, and C — preliminary or tentative. Typical use cases of visual orbits are listed. Accurate parallaxes from Gaia, together with the orbits, will greatly expand the data on stellar masses. Continued speckle monitoring will be an essential complement to Gaia, but the vast amount of new pairs will restrict future work on orbits to the most interesting or relevant objects.

Keywords: binaries:visual

1. INTRODUCTION

Orbital motion of resolved binary stars, by tradition called “visual”, is evidenced by change of their relative positions over time. When the measurements cover a substantial fraction of the orbit, its seven elements can be determined. The orbit calculation has been a classical problem in astronomy for over two centuries, and its solution is well covered in papers and textbooks (Aitken 1935; Heintz 1978). At first glance, this is a classical data modeling problem where standard methods are applicable. However, several aspects present specific challenges, namely the non-linear relation between data and parameters, an insufficient coverage, and unreliable or ambiguous measurements. The methods of orbit computing have evolved over time, driven by the increasing computing power and better data, so most textbook methods have nowadays become obsolete. New methods emerge, mostly based on statistical approaches and tailored to particular needs, e.g. orbits of directly imaged exoplanets (Stojanovski & Savransky 2024) or a dynam-

ical analysis involving radial velocities (RVs) and accelerations (Brandt et al. 2021).

In this work, I share my experience of computing orbits of relatively close resolved pairs using both historic visual measurements and modern speckle interferometry, and formulate several recommendations. The current approach to orbit fitting, described by Hartkopf et al. (2001), is revised here because the quality and quantity of the input data is steadily improving owing to the ongoing speckle interferometry programs and other techniques such as adaptive optics and long-baseline interferometers. The role of the old visual data diminishes correspondingly. Typical “visual” binaries are nowadays closer and move faster than in the epoch of visual measures. In the past, partial coverage of a long-period orbit was a major obstacle, and methods of computing orbits from short observed arcs were given particular attention. Now we often face the opposite situation when the orbit is not known even after covering several periods because the existing measurements are not frequent enough. A similar problem occurs in fitting astrometric and spectroscopic orbits to the Gaia data (Gaia Collaboration et al. 2021) because the temporal sampling is determined by the satellite’s scanning law,

and nothing can be done to modify it (Halbwachs et al. 2023; Holl et al. 2023).

The quality and reliability of the input data is the main reason why the orbit computing is so special; it precludes automatic orbit determination, which would otherwise appear attractive. The relative positions measured visually should be treated as estimates rather than as real measurements with known errors. Modern speckle measurements also need a critical assessment. Piecing together incomplete information makes calculation of some visual orbits a challenging task. Unreliable or insufficient data often lead to poorly constrained or plainly wrong orbits.

The input data used for orbit determination and the methods of fitting Keplerian orbits are reviewed briefly in Section 2. A simplified system of three grades is proposed, replacing the obsolete 5-grade classification tailored to the quality of the old data. The science resulting from visual orbits is outlined in Section 3. Section 4 illustrates important aspects of orbit calculation by examples taken from my current work. Section 5 formulates recommendations based on my experience and discusses future trends.

2. ORBIT CALCULATION

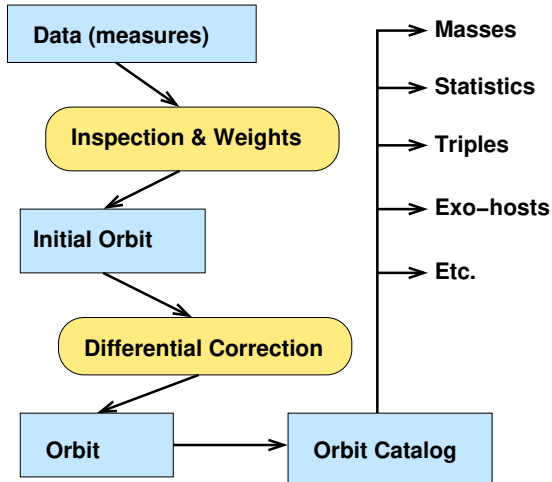


Figure 1. Flow chart of orbit calculation.

The methods of orbit calculation have evolved over two centuries. A multitude of historic orbit-computing methods (Aitken 1935), invented to alleviate the burden of calculus, nowadays are obsolete. Here, the modern approach to orbit calculation, illustrated by the flow chart in Figure 1, is outlined.

2.1. Position Measurements

When the input data (position measurements, also called *measures*) are reliable and sufficient, their mod-

eling (fitting an orbit) presents no difficulty and can be handled without human supervision. However, these conditions are rarely met in practice. Understanding the input data and their limitations is of critical importance to orbit calculation. For this reason, most orbits were and still are computed by the same people who produce the data. Orbit calculation and improvement is the primary motivation for monitoring the motion of visual binary stars.

Most double-star measures were made in the 19th and 20th centuries visually. This technique is sometimes called filar micrometer. Visual measures of close pairs rely on the real-time image analysis by human brain that resembles speckle interferometry (Couteau 1978; Heintz 1978). These measures are always subjective. Typically, separations are estimated with larger relative errors than position angles. After correction of the systematic overestimation of separations, the measurements by the experienced visual observer, P. Couteau, show random errors of $0''.03$ (Tokovinin 1983). The errors of visual measures are not provided by their authors, and the fraction of discrepant measures and spurious visual resolutions is substantial.

Hartkopf et al. (2001) present a thorough statistical evaluation of the errors of visual measures, estimated a posteriori from their residuals to the orbits. They parametrize the errors by the diffraction limit λ/D of the telescope used (λ is the wavelength and D is the aperture diameter), with coefficients depending on the experience of each observer and the number of averaged measures. Their Figure 4 indicates typical residuals of $0''.07$ and relative residuals in separation of $\sigma_\rho/\rho \sim 0.12$, with a large scatter and no obvious dependence on the orbit quality. Orbits were typically based on 20–100 such measures (or, better said, estimates).

Almost two centuries of visual double-star observations created a legacy data set assembled in the Washington Double Star (WDS) catalog (Mason et al. 2001).¹ We are indebted to the observers of the past and use their data as a “time machine” that traces orbital motions back in time. Nowadays, most measurements are made using speckle interferometry at large or moderate-size telescopes. Other methods (long-baseline interferometers, adaptive optics, ground- and space-based astrometry) are also relevant. Their review is outside the scope of this paper.

Here I use mostly speckle measures made at the 4.1 m Southern Astrophysical Research (SOAR) telescope using the HRCam instrument (Tokovinin et al. 2010;

¹ <https://crf.usno.navy.mil/wds/>

Tokovinin 2018a); the latest papers (Mason et al. 2023; Tokovinin et al. 2024) give references to prior publications of the results. As of May 2024, the HRCam database contained 27,184 measurements of relative positions. The pixel scale and orientation are calibrated by observing slowly moving binaries with separations on the order of $1''$; this calibrator set was referenced to Gaia in Tokovinin et al. (2022), and the recommended minor corrections to the measures made before 2021 (subtract 0.2 from the position angles and divide the separations by 1.0053) are applied here. For most binaries, residuals of the HRCam positions from the orbits are within 2 mas, so such errors are assumed. The less accurate speckle measures at 4 m telescopes by CHARA and other teams are given here errors of 5 mas. Note that the weighting system adopted by Hartkopf et al. (2001) accounts for the smaller speckle errors only by the aperture-size factor λ/D . So, a typical 70 mas error of visual measures with 0.7 m telescopes corresponds to 12 mas with 4 m telescopes, and this weighing scheme severely under-estimates the real accuracy of the speckle data relative to the visual measures.

When the magnitude difference Δm is small (i.e. the components' fluxes are comparable), the position angle can be “flipped” by 180° . The classical speckle interferometry yields angles modulo 180° for all binaries, although this ambiguity can be removed using advanced techniques such as image restoration when Δm is not too small. The quadrant ambiguity sometimes presents substantial problems, as illustrated by the examples below.

2.2. Orbital Elements

Motion of a resolved binary system is described by the seven classical Campbell orbital elements: period P , time of periastron passage T , eccentricity e , semimajor axis a in angular units, position angle of the ascending node Ω , longitude of the periastron from the ascending node ω , and orbital inclination i (Aitken 1935; Heintz 1978; Brandt et al. 2021). If radial velocities (RVs) of the primary and secondary components are measured, their amplitudes K_1 and K_2 and the systemic velocity γ can be determined, increasing the total number of orbital elements to ten.

For pairs with direct (counterclockwise) motion, the inclination $i < 90^\circ$, for the retrograde (clockwise) motion $90^\circ < i < 180^\circ$. Face-on orbits with $i \approx 0^\circ$ or $i \approx 180^\circ$ are degenerate because the elements Ω and ω are strongly correlated (both define orientation of the orbital ellipse on the sky). In such case, it is appropriate to set $\omega = 0$ and to fit the remaining five elements. Circular orbits with $e \approx 0$ are also degenerate because

the periastron is arbitrary; by setting $\omega = 0$, we effectively redefine the element T as the time of the nodal passage. In a circular face-on orbit, T and Ω also become degenerate, and only three elements P, T, a suffice to describe the motion (in such case, T is the time when $\theta = 0$).

2.3. Orbit Determination

Let $x_k(t_i)$ be the measurements, e.g. the position angle θ and separation ρ at time t_i or, alternatively, the offsets of the companion in declination and R.A. ($k = 1, 2$). The measurement errors are $\sigma_{k,i}$. The vector of the seven orbital elements \mathbf{p} (parameters) determines the ephemeris positions $\hat{x}_k(t_i, \mathbf{p})$. Deviations of measurements from the orbit (residuals) are characterized by the standard χ^2 metric,

$$\chi^2 = \sum_{i,k} \frac{[x_k(t_i) - \hat{x}_k(t_i, \mathbf{p})]^2}{\sigma_{k,i}^2}. \quad (1)$$

Fitting an orbit to measurements implies finding the parameters \mathbf{p} that minimize χ^2 — a typical data-modeling problem. This approach can be extended by including additional types of data, such as RVs (Pourbaix 2000; Lucy 2018) and/or accelerations (Brandt et al. 2021); however, additional parameters (e.g. masses, distances, or RV amplitudes) must be fitted in such cases. This formulation assumes implicitly that the measurement errors $\sigma_{k,i}$ are known and normally distributed, which is not quite true for position measurements, especially those made visually. Nevertheless, this approach with suitably assigned errors is universally adopted. Evaluation of the errors (which are either not published together with the measures or are only lower limits) is the cornerstone of the orbit computing: different orbits are derived from the same data by adopting different errors.

The specifics of fitting a visual orbit is the high dimensionality of the parameter space, the diversity of situations, depending on the orbit orientation and its coverage, and the non-linear relation between parameters and data. The latter aspect can be partially improved by replacing the Campbell elements a, Ω, ω, i by their combinations A, B, F, G , called the Thiele-Innes (T-H) elements (Aitken 1935; Heintz 1978). Linear relation between the T-H elements and the measurements allows us to solve the least-squares (LS) problem by the standard matrix method, but the remaining non-linear elements P, T, e need to be known to take advantage of this parametrization.

The high dimensionality of the parameter space and the non-linearity, combined with insufficient data, often result in a complex topology of the χ^2 surface with multiple local minima. The shape of this hypersurface also

depends on the adopted errors $\sigma_{i,k}$ and is strongly influenced by the highly deviant or wrong measurements. These aspects make the orbit fitting a tricky problem. If the orbital elements are known approximately (e.g. from prior work), they can be corrected (improved) via linearization and LS fitting. So, finding an initial approximation of an orbit is the first and critical step.

2.4. Initial Approximation

An obvious approach to finding the global χ^2 minimum is to split the parameter space into the linear and non-linear domains. This is implemented in the *grid search* method (Hartkopf et al. 1989). A suitably fine grid in the 3-dimensional space of the non-linear parameters P, T, e is defined and explored by brute force. At each grid point, the T-H elements are fitted, and the grid point with the minimum χ^2 is taken as the initial approximation for the final LS refinement of all elements.

The grid search method is perfect for reliable data. However, rejection (or down-weighting) of poor data is a critical step in orbit fitting. Furthermore, flips of the position angles by 180° , when allowed, critically affect the orbit. So, instead of relying on the blind grid search, I examine the input data and find the initial approximation heuristically.

The third Kepler law gives a crude estimate of the orbital period P^* (in years) as

$$P^* = (\rho/\varpi)^{3/2} M^{-1/2}, \quad (2)$$

where ρ is the typical separation, identified with the semimajor axis a , ϖ is the parallax, and M is the mass sum in solar units. The parallaxes are nowadays known from Gaia or, otherwise, can be estimated photometrically assuming main-sequence stars; $M = 2 \mathcal{M}_\odot$ is a good starting assumption. Statistically, the condition $\rho \approx a$ holds within a factor of 2, and the crude estimates P^* typically differ from the true periods within a factor of ~ 3 .

I use the interactive IDL code `orbit` (Tokovinin 2016) to plot the measurements and to find the initial approximation. At this stage, the outliers are rejected and the quadrant flips are adjusted. The sense of the orbital motion suggests to start with $i = 60^\circ$ (counterclockwise) or $i = 120^\circ$ (clockwise); the time of the closest approach gives an idea of the periastron epoch T , the position angle at maximum separation gives Ω , assuming $\omega \approx 180^\circ$, $P = P^*$, $a = \rho$, and $e = 0.5$. A few manual tweaks of the crude starting elements usually suffice to get an initial orbit that resembles the data approximately. If the separation remains almost constant, we can start with a circular orbit by setting $e = \omega = 0$, and allow a non-zero eccentricity later in the LS fit. If the LS solution con-

verges to a negative e , make the following replacements: $T \rightarrow T \pm P/2$, $\omega \rightarrow \omega \pm 180^\circ$, $e \rightarrow -e$.

It is often helpful to reduce the dimension of the parameter space by fixing most elements and fitting only one or two. In this way, the initial orbit can be made closer to the data. Experience helps us to decide which elements need to be fitted or changed manually at this initial stage to get a reasonable first approximation. Sometimes the data can match several radically different orbits (Section 4.5).

2.5. Orbit Correction

The final adjustment of the orbital elements is done by the standard iterative LS method, linearizing the model in the vicinity of the initial parameters \mathbf{p}_0 :

$$\hat{x}_k(t_i, \mathbf{p}) \approx \hat{x}_k(t_i, \mathbf{p}_0) + \sum_j \frac{\partial \hat{x}_k(t_i, \mathbf{p})}{\partial p_j} (p_j - p_{0,j}), \quad (3)$$

where the index j denotes the fitted parameters. The partial derivatives of the Keplerian orbit can be calculated analytically or numerically (the latter approach is used in `orbit`, while analytic gradients were programmed in its earlier FORTRAN version). The linearization allows minimization of χ^2 by the standard Levenberg-Marquardt method which combines the steepest descent with the full LS solution (Press et al. 1986). The formal errors of the fitted elements and their covariances are determined in the process, as well as the goodness of fit metric χ^2 . If the data errors are assigned correctly, we expect to obtain $\chi^2/(N - J) \approx 1$ for N measurements and J fitted parameters. This metric is computed separately for each type of data (e.g. separations and angles) specified by the index k .

As noted above, in some cases the set of orbital elements is degenerate (the matrix of the corresponding LS problem is singular), so some elements (or their combinations) must be fixed. Often the data do not constrain the elements well enough. For example, a short observed arc does not constrain the period P and the semimajor axis a . However, these elements are usually strongly correlated, so their ratio a^3/P^2 that defines the mass sum is constrained much better than P and a (Lucy 2014). Another typical situation is when the binary is not resolved at close separations near the periastron of an eccentric orbit, so the data match a range of eccentricities e . If the parallax is known, calculation of the mass sum by the third Kepler's law and its comparison with the expected masses helps us to select values of poorly constrained elements. Generally speaking, the mass sum is a good sanity check for all orbital solutions.

Typically, new measurements are used to improve known orbits by differential correction. However, if the

initial (old) orbit is wrong, the differential correction will not change it dramatically, and the updated orbit will remain wrong as well. In such cases, a new initial orbit is needed, and the orbit calculation must be restarted from scratch.

2.6. Orbit Catalog and Grades

Data on all visual orbits are assembled in the electronic catalog ORB6 maintained at USNO² and described by Hartkopf et al. (2001). The quality of visual orbits was traditionally estimated by experts, with grade 1 for the best and grade 5 for the worst (tentative) orbits. The subjective grades were replaced by the automatic grading system developed by Hartkopf et al. (2001). At that time, most orbits were still based on the visual data, so the grading algorithm was tailored to this reality and “trained” on the subjective grades assigned by the experts. For example, a large number of measurements was required for grade 1 orbits, although only ~ 10 accurate positions with a good phase coverage suffice for computing an accurate orbit. A simple one-dimensional grading scheme cannot capture the diversity of situations and the multi-dimensional nature of the orbital parameters. What really matters are the errors (i.e. the confidence intervals) of the elements or, more generally, the constraints provided by the data. I propose to replace the existing orbit grades by a simple 3-tier classification:

- *Grade A* — fully constrained orbits with meaningful estimates of the errors (or confidence intervals) for all elements. The orbit quality is characterized by the errors better than by the discrete grades.
- *Grade B* — semi-constrained orbits where the error of the period is determined, but one or more other poorly constrained elements can be fixed in the orbit fitting.
- *Grade C* — unconstrained or preliminary orbits (this corresponds roughly to the old grades 4 and 5). No meaningful estimates of the elements’ errors can be given.

The low reliability of visual measures has been generally recognized, and traditionally the observers were not blamed for producing deviant data points or spurious resolutions. The visual orbits based on these data inherited the culture of error tolerance which differs markedly from the more strict attitude to spectroscopic orbits. Another justification for publishing low-quality or tentative orbits is related to the long orbital periods. A

tentative orbit estimated from the short observed arc may be completely off, but it is still better than nothing, with little prospect of improvement in the following decades owing to the slow motion. In the ORB6 catalog (queried on 2024 August 1), 1816 orbits (59%) are of grades 4 and 5 (preliminary and tentative), and only 1340 orbits of grades 1, 2, and 3 are more or less reliable.

In his paper “Is this orbit really necessary?”, van den Bos (1962) questioned the established practice of publishing poorly constrained low-grade orbits. He also argued that well-defined orbits should not be revised in response to new measures. However, the high accuracy of speckle interferometry calls for the correction of even the best old orbits which were based on the less accurate historic data. I agree that such corrections should not be too frequent, they should be justified by the well-established systematic residuals to the existing orbits. Two such examples are given below in Section 4.1.

Publication of orbits poorly constrained by the currently available data can be justified by their subsequent use. Tentative orbits represent the existing measures and help in planning future observations (e.g. predict the critical phases near periastron). They serve for computing past and future positions on the sky (improve the coordinates by accounting for the orbital motion), and are valuable for the study of stellar systems that contain additional bodies (e.g. inner subsystems, disks, or exoplanets). A high demand for evaluating orbital parameters even from short arcs prompted the development of new methods and software (Blunt et al. 2020; Brandt et al. 2021).

Owing to the ongoing speckle programs, the content of the ORB6 in terms of the number of orbits and their quality is steadily improving. We should keep in mind, however, that the knowledge of visual orbits does not advance the science by itself, but rather serves as a fundamental basis for further research, as outlined in the following Section.

3. USE OF VISUAL ORBITS

Discovery of double stars by visual resolution, their monitoring, and calculation of orbits based on the accumulated measures is the classical pattern. This research program has been executed for two centuries by several generations of astronomers. Its continuation (compute new orbits and improve the existing ones) appears natural. Without orbits, the past measures remain essentially useless, so monitoring of “everything that moves” seems to be an adequate tribute to our predecessors, extending their effort into the future. However, the use of the telescope time and other resources cannot be justi-

² <https://crf.usno.navy.mil/wds-orb6/>

fied only by the need to improve the ORB6 catalog: by itself, it does not produce new science. The current use of visual orbits is reviewed below.

3.1. Measurement of Masses

Historically, visual orbits served to measure stellar masses, to establish the mass-luminosity relation, and to test stellar evolutionary models (Andersen 1991). For the latter, a relative accuracy of the mass on the order of 2% or better is considered adequate. The mass sum of a visual binary M is computed by the third Kepler law expressed by equation 2, where P^* and ρ are replaced by the true period P and the semimajor axis a , respectively:

$$M = (a/\varpi)^3 P^{-2}. \quad (4)$$

Only a minority of very good orbits in ORB6 have the quantity a^3/P^2 precise enough for useful tests of evolutionary models. Moreover, the parallax ϖ must be known with a matching accuracy of 0.6%, and here we have a problem. About two thirds of objects in ORB6 do not have any astrometry in Gaia DR3 (Chulkov & Malkov 2022), while the Hipparcos parallaxes are not accurate enough. For the remaining orbital binaries, the Gaia DR3 does not account for the orbital motion while fitting the standard 5-parameter astrometric solutions, so the parallaxes of most visual binaries are biased. The bias is corrected only for binaries with astrometric orbits in Gaia; their periods are shorter than 3 yr (Halbwachs et al. 2023).

There are several ways to circumvent the Gaia limitations concerning visual binaries. When a visual binary is accompanied by a distant bound tertiary companion, its accurate Gaia parallax can be used for measuring the masses (see for example 00024+1047 in Section 4.5). Alternatively, the Gaia data on individual transits, which will become public in the next data release DR4, can be used in combination with the speckle measures to fit both the astrometry and the orbit jointly. The ORVARA code (Brandt et al. 2021) is a suitable tool for doing this. Finally, the combination of visual and double-lined spectroscopic orbits yields distances and masses directly without the need of astrometric parallaxes (Pourbaix 2000); however, a very high accuracy of both resolved measures and RVs is mandatory for accurate mass measurement.

The majority of visual binaries with known orbits have solar-type components, and masses of such stars are already known quite well, so additional similar data have little value. The current interest focuses on less explored stars, for example on the M-type dwarfs (Mann et al. 2019; Vrijmoet et al. 2022), brown dwarfs (Rickman et al. 2024), pre-main se-

quence stars (Rizzuto et al. 2020), or very massive stars (Schaefer et al. 2016; Klement et al. 2024). In these cases, even modestly accurate masses contribute new knowledge.

3.2. Statistics

A catalog of orbits can be exploited for statistical studies. One of the classical topics is the period-eccentricity relation. Analysis of spectroscopic and visual orbits established a trend of increasing mean eccentricity with increasing period (Finsen 1936; Tokovinin & Kiyaveva 2016). Using the Gaia data, the eccentricity distribution of very wide binaries was evaluated statistically, confirming and extending this trend to large separations (Hwang et al. 2022).

The major obstacle in using ORB6 for the statistics is its heterogeneous and random content. The calculation of an orbit is driven by the data availability, which varies greatly, as can be inferred from the examples in this paper. Very eccentric orbits are particularly demanding in this respect, and they are under-represented in the catalogs (so-called Finsen’s effect, Finsen 1936). A large fraction of low-grade orbits and their drastic revisions reduce the confidence in the distributions of periods or eccentricities derived from ORB6. To overcome these caveats, one can restrict the input samples, for example to solar-type stars within 25 pc (Raghavan et al. 2010) or to nearby M-type dwarfs (Vrijmoet et al. 2022). In these smaller samples, the completeness of known visual orbits can be tested, and additional observations can be planned to improve it.

The orbital angles Ω, ω, i are not interesting in their own right because binary orbits are oriented randomly. However, the orbital inclinations serve to probe relative alignment of orbits with stellar spins (Weis 1974), with orbits of transiting exoplanets (Lester et al. 2023), or with inner subsystems in stellar hierarchies (Tokovinin 2017, 2021a). Although the content of ORB6 is highly heterogeneous, these studies postulate that the calculation of visual orbits is not influenced by the orientation of stellar axes or planetary orbits, hence any revealed correlations are genuine.

3.3. Hierarchical Systems

Hierarchical systems of three or more stars have a diverse architecture related to their formation and early evolution (Tokovinin 2021b; Offner et al. 2023). Relative orientation of inner and outer orbits in triple systems, period ratios, mutual dynamics, and potential resonances present a rich research field where calculation of orbital elements plays an essential role (Borkovits et al. 2016).

As an example, consider HIP 12548, a classical visual binary discovered by R. Aitken in 1931 and composed of solar-type stars. Historic measures, complemented by the speckle interferometry, define its 106 yr orbit quite well. However, spectroscopic monitoring revealed that each visual component has a variable RV, so this is a 2+2 quadruple system with inner periods of 5.07 and 0.30 yr (Tokovinin 2022). The 5 yr subsystem produces measurable deviations (wobble) in the positions, allowing us to establish the relative orientation of the subsystem with respect to the outer orbit. This case resembles the classical visual binary α Gem (Castor), where each visual component is a close spectroscopic pair. Recently, both spectroscopic subsystems in Castor were spatially resolved by the CHARA interferometer, showing that the inner orbits are not aligned with the outer visual orbit (Torres et al. 2022). In both cases, the classical visual binaries are revealed as hierarchical systems, and their orbits acquire new significance. Needless to say that using such visual pairs for testing stellar evolution makes no sense without measuring masses of all components, because they are not simple binaries.

3.4. Objects of Special Interest

Calculation of visual orbits is required for various reasons when the stars present some special interest or significance. A typical case are exohosts, where the knowledge of orbits constraints the size of truncated protoplanetary disks and thus informs us on the planet formation mechanisms or, statistically, probes the relative alignment between transiting planets and the orbits of their hosts (Lester et al. 2023). The orbital motion of directly imaged planets is being monitored, and even short observed arcs help to evaluate the range of possible orbital parameters (Stojanovski & Savransky 2024).

The pre-main sequence (PMS) star HD 98800 is a 2+2 quadruple system where the outer pair A,B is a classical visual binary I 507 (11221–2447). Recent interferometric observations have established the orientation of the inner subsystems relative to the outer orbit (Zúñiga-Fernández et al. 2021). The inner pair Ba,Bb is

surrounded by a debris disk which is nearly perpendicular to its orbit. The A,B pair is closing down, and during the upcoming conjunction in 2026–2027 the disk will occult the subsystem Aa,Ab, offering a unique chance to study the detailed disk structure by photometric monitoring of the occultation. The knowledge of the outer orbit is critical for interpretation of these data, and the historic visual measures of A,B play an important role here.

Yet another emblematic case is the Cepheid Polaris (α UMi), member of a triple system. The orbit of the inner 30 yr subsystem determined using RVs and resolved measures yields the Cepheid mass (Evans et al. 2024). Owing to the large magnitude difference, the position measures come from telescopes in space or from the long-baseline interferometry; this “visual” binary is beyond the reach of classical visual observers of the past.

4. EXAMPLES OF ORBITS

The specifics of the visual orbit calculation and the associated caveats are illustrated here with 20 orbits recently computed or revised by the author. We start with two accurate and very well-constrained orbits based on both visual and speckle data, followed by several examples of orbits relying entirely on the speckle measurements. Then two interesting cases illustrating spurious visual resolutions of very close pairs are presented. Examples of dramatic revisions of published orbits and a few tentative first-time orbits close this Section. The orbital elements and their errors are listed in Table 1. Table 2, available in full only electronically, contains all measurements, their adopted errors, and the residuals to the orbits. According to the rules adopted in the Washington Double Star Catalog, WDS (Mason et al. 2001), each binary is identified by its WDS code based on the J2000 position and by a unique string called “Discoverer Designation” (DD); the DDs, however, are barely used outside the double-star community. In hierarchical systems, a common WDS code refers to several pairs with different DDs. An alternative designation scheme based on components, rather than pairs, is adopted in the Multiple Star Catalog (Tokovinin 2018b).

Table 1. Visual Orbits

WDS	Discoverer	P	T	e	a	Ω	ω	i	Grade	Previous
	Designation	(yr)	(yr)		(arcsec)	(deg)	(deg)	(deg)		Orbit ⁴
00024+1047	A 1249 AB	58.86	2002.91	0.806	0.2004	66.4	18.6	110.6	A	Zir2003
		± 1.25	± 0.55	± 0.022	± 0.0031	± 2.2	± 5.9	± 1.4		

Table 1 continued

Table 1 (*continued*)

WDS	Discoverer	P	T	e	a	Ω	ω	i	Grade	Previous
	Designation	(yr)	(yr)		(arcsec)	(deg)	(deg)	(deg)		Orbit ⁵
04123+0939	STT 74	110.09	1996.83	0.905	0.3332	111.9	17.0	108.8	A	Msn2019
		± 1.81	± 0.30	± 0.006	± 0.0038	± 0.9	± 2.6	± 0.8		
04386-0921	TOK 387	4.239	2019.351	0.450	0.0509	40.6	292.9	106.2	A	...
		± 0.035	± 0.043	± 0.028	± 0.0014	± 1.1	± 2.7	± 1.7		
05005+0506	STT 93	3200	1913.563	0.80	4.108	60.6	65.5	100.3	C	Izm2019
05251-3803	I 1493	250	2045.0	0.70	0.238	153.2	92.7	57.2	C	...
10407-0211	A 1351	168.7	1992.87	0.90	0.4742	74.2	250.1	115.2	C	...
13453+0903	BU 115 AB	800	2164.4	0.50	1.793	103.3	264.8	55.2	C	Izm2019
14056-3916	I 1575	64.9	2018.62	0.776	0.1353	119.5	290.8	160.0	C	...
14160-0704	HU 138	142.8	1938.26	0.571	0.4477	74.3	304.9	43.5	A	Doc1990d
		± 2.8	± 0.69	± 0.016	± 0.0068	± 2.9	± 1.9	± 1.9		
14453-3609	I 528 AB	15.933	2023.555	0.593	0.0459	236.5	66.6	25.6	A	Tok2022f
		± 0.162	± 0.090	± 0.028	± 0.0023	± 18.5	± 17.3	± 7.7		
15493+0503	A 1126	1000	2005.83	0.90	0.291	16.2	8.6	38.6	C	Gomez2022
16090-0939	WSI 85	9.51	2020.89	0.97	0.0986	139.4	319.2	83.8	B	...
		± 0.15	± 0.30	fixed	± 0.0273	± 3.4	± 19.2	± 5.2		
16103-2209	TOK 860	7.72	2023.10	0.314	0.0479	121.2	111.9	95.9	A	...
		± 0.60	± 0.15	± 0.078	± 0.0013	± 1.5	± 10.6	± 1.5		
16245-3734	B 868 AB	1.700	2022.711	0.957	0.0194	164.9	299.7	20.0	B	...
		± 0.014	± 0.083	± 0.098	± 0.0114	± 696.2	± 674.2	fixed		
16520-3602	RSS 420 Aa,Ab	6.99	2018.503	0.40	0.0979	18.6	103.0	139.5	B	...
		± 0.06	± 0.057	fixed	± 0.0013	± 3.6	± 2.1	± 1.4		
17005+0635	CHR 59	13.111	2014.45	0.725	0.1063	65.6	187.7	24.9	A	Tok2022f
		± 0.056	± 0.16	± 0.032	± 0.0025	± 26.6	± 29.5	± 10.9		
17093-2954	B 330	57.75	1998.26	0.353	0.1780	65.2	126.5	45.6	A	...
		± 1.46	± 0.75	± 0.027	± 0.0085	± 3.8	± 5.8	± 3.7		
17304-0104	STF2173 AB	46.538	2008.715	0.175	0.9697	151.63	325.56	99.33	A	Msn2023
		± 0.019	± 0.042	± 0.001	± 0.0008	± 0.04	± 0.35	± 0.04		
17305-1006	RST3978	93.93	2008.60	0.244	0.5737	97.0	91.0	78.3	A	Tok2015c
		± 2.03	± 0.44	± 0.019	± 0.0055	± 0.2	± 2.8	± 0.3		
19164+1433	CHR 85 Aa,Ab	6.938	2022.495	0.577	0.0392	37.5	148.5	147.4	A	Tok2015c
		± 0.023	± 0.083	± 0.021	± 0.0011	± 8.9	± 10.8	± 6.0		

^aReferences to previous orbits: Doc1990d = Docobo & Costa (1990); Gomez2022 = Gómez et al. (2022); Izm2019 = Izmailov (2019); Msn2019 = Josties & Mason (2019); Msn2023 = Mason et al. (2023); Tok2015c = Tokovinin et al. (2015); Tok2022f = Tokovinin et al. (2022); Zir2003 = Zirm (2003)

4.1. Accurate Orbits

Orbits of classical visual binaries are computed and recomputed many times until they become “definitive”. Even then, some adjustments may be needed. Two relevant cases are illustrated in Figures 2 and 3.

The pair 14160-0704 (HU 138) has been discovered by Hussey in 1900.3; by now, it has almost completed one revolution of its 143 yr orbit. The latest orbit by Docobo & Costa (1990) had a period of 151.4 yr. Accurate positions are available for the period 1989.3–2024.15. The magnitude difference measured at SOAR

is small, about 0.2 mag, but sufficient to establish that the secondary is located in the south-west quadrant, differing from the ephemeris by 180° . The relative position of the companion in Gaia DR3 confirms the quadrant, with $\Delta G = 0.13$ mag. So, the Docobo’s orbit should be “flipped” (change Ω by 180°), and all visual measures should be flipped as well. Alternatively, we can keep the historic identifications of the primary and secondary stars in this system, flip the modern measures, and assign them a negative Δm . Apart from the flip of the Docobo’s orbit, one notes its systematic deviation from the latest measures. This justifies the small correction of the elements made here. The deviant speckle measure in 1996.42 was given a reduced weight. The period of 143.0 ± 2.7 yr is well established, but in the future this “definitive” orbit will need further minor adjustments

Table 2. Positional Measurements and Residuals (Fragment)

WDS	T	θ	ρ	σ	$O-C_\theta$	$O-C_\rho$	Ref. ^a
	(yr)	($^\circ$)	($''$)	($''$)	($^\circ$)	($''$)	
00024+1047	1905.5500	239.9	0.3300	0.0500	-3.6	-0.0053	M
00024+1047	1916.2100	236.2	0.3400	0.0500	-2.7	-0.0014	M
00024+1047	1926.7400	227.4	0.2800	0.0500	-6.0	0.0063	M
00024+1047	1979.7400	235.8	0.2900	0.0500	-1.0	-0.0305	M
00024+1047	1987.7532	231.3	0.2520	0.0050	-0.5	0.0017	s
00024+1047	1988.6595	231.0	0.2400	0.0050	-0.0	0.0006	s
00024+1047	1991.2500	218.0	0.1850	0.0500	-10.3	-0.0194	H

^a A: adaptive optics; G: Gaia; H: Hipparcos; M: visual micrometer measurement; S: speckle interferometry at SOAR; s: speckle interferometry at other telescopes.

(This table is available in its entirety in machine-readable form)

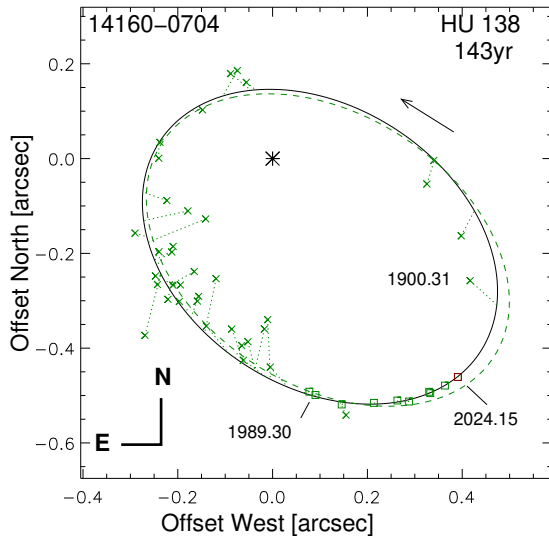


Figure 2. The definitive orbit of 14160–0704 (HU 138). In this and following plots, the primary component is located at the coordinate origin, the axis scale is in arcseconds (North up, East left). The accurate measurements are plotted as squares (in red color after 2023.0), the less accurate (e.g. visual) ones as crosses. The full line is an orbital ellipse, the dashed line plots the previously computed orbit.

as the visual coverage is progressively replaced by accurate relative positions. Until then, the historic visual measures will remain critical for constraining this orbit.

The classical visual binary 17304–0104 (STF 2173) was discovered by W. Struve in 1829 at $0''.6$ separation and since then has completed four revolutions of its 46 yr orbit. The latest adjustment of the elements using all available data was published recently by Mason et al. (2023). As shown in Figure 3, right, this orbit (dashed line) has minor but systematic residuals from the speckle measures, which started in 1977.3 and now cover one full revolution. I corrected the orbit using only the 89

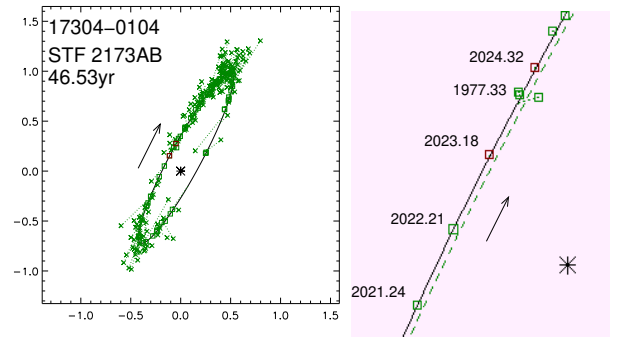


Figure 3. The accurate speckle-only orbit of 17304–0104 (STF 2173) on the left, with the visual measurements in the 19th century overplotted as crosses. Its fragment on the right shows the systematic residuals to the previous orbit (dashed line).

speckle positions and the 29 RVs from Pourbaix (2000). The weighted rms residuals are 4.4mas , the period is 46.538 ± 0.019 yr. In this case, using a large number of visual positions, even with low weights, degrades the orbit accuracy instead of improving it. If I include, for a test, several early visual measures in the LS fit, the error of the period decreases insignificantly, to 0.018 yr (the full-orbit speckle coverage constrains the period quite well). The left panel of Figure 3 illustrates the situation by overplotting visual measures made before 1900. Effectively, these data contribute only noise. So, when the micrometer measures are not absolutely necessary for the orbit calculation (as is the case here), it is better to ignore them.

4.2. Speckle-Only Orbits

On average, binary stars discovered by speckle interferometry are closer than classical visual binaries. So, they move faster, allowing calculation of orbits with pe-

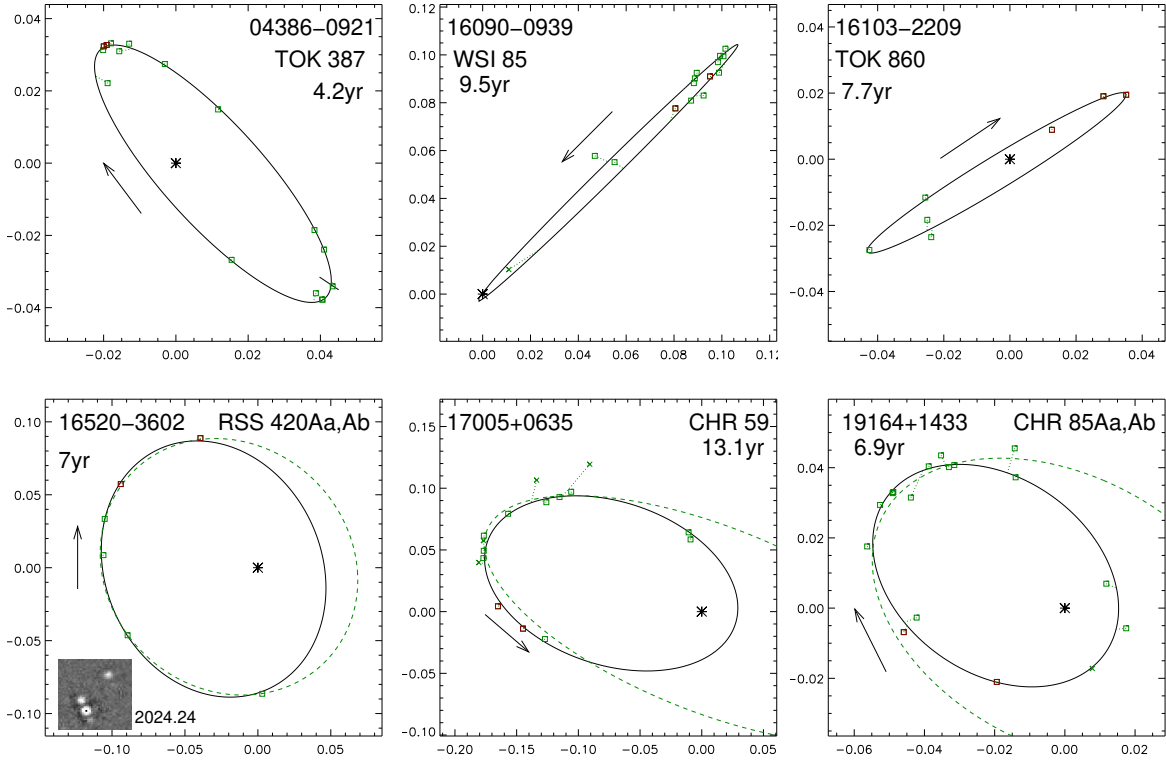


Figure 4. Six orbits based only on speckle measurements. The WDS codes, discoverer designations, and periods are indicated. Alternative orbits are plotted by dotted lines.

riods on the order of a decade. Six such orbits are illustrated in Figure 4 and commented below.

04386–0921. The pair was resolved at SOAR in 2014; it has completed 2.4 revolutions, and the orbit with $P = 4.239 \pm 0.035$ yr determined from 16 measures made exclusively at SOAR is tightly constrained. The rms residuals are only 1 mas. The small magnitude difference $\Delta m \sim 0.5$ mag and the spectral type F8V favor measurements of the RVs for both components, so a combined spectro-interferometric orbit can be determined in the future if the pair is monitored spectroscopically.

16090–0939. This bright ($V = 7.24$ mag) A8V star HIP 79122 was resolved for the first time in 2008 at the 4 m Blanco telescope using HRCam (Tokovinin et al. 2010). A substantial magnitude difference of $\Delta m \sim 3.5$ mag and the large eccentricity conspire to prevent resolution of this pair near the periastron (the cross in the orbit plot marks the non-resolution in 2021.3), so this important part of the orbit is not covered and the eccentricity is not well constrained. In the orbit fit, I fixed $e = 0.97$ to get a mass sum of $5.3 M_{\odot}$ with the Gaia DR3 (Gaia Collaboration et al. 2021) parallax of 12.57 ± 0.09 mas. An unconstrained fit converges to $e = 0.99$ and corresponds to the excessive mass sum of $16 M_{\odot}$. The residuals are 2.2 mas. A large RV variation around the next periastron in 2030.4 is expected.

16103–2209. This star, HIP 79244 (spectral type A0V), was resolved at SOAR in 2019. Six measurements made to date (plus two non-resolutions in 2022) constrain the 7.7 yr orbit reasonably well; it yields a mass sum of $7.6 M_{\odot}$ with the Gaia DR3 parallax of 6.26 ± 0.09 mas. In 2023.18, the separation of 15.5 mas (under the diffraction limit) was estimated by fixing Δm . Additional measurements are needed to confirm and improve this orbit.

16520–3602. This relatively faint ($V = 12.0$ mag) M2V dwarf HIP 82521 (NLTT 43673) was resolved in 2019 into a tight triple with separations of $0''.09$ and $0''.4$ (the insert in Figure 4 shows the latest shift-and-add image of the triple). In the WDS, these pairs received the DDs designations RSS 420Aa,Ab and RSS 420AC, respectively. Note, however, that the faint companion B at $6''.6$ which gave rise to the original RSS designation is unrelated according to the Gaia astrometry. The separations in this triple and the Gaia DR3 parallax of 26.76 ± 0.31 mas imply the inner and outer orbital periods P^* of a few and ~ 50 yr, respectively. After five years of monitoring, the first 7 yr orbit of the inner pair can be determined. The unconstrained orbit fit gives $e = 0.22 \pm 0.11$ and a mass sum of $0.64 M_{\odot}$ (dashed line in Figure 4), while the luminosity and the spectral type of these stars correspond to a mass sum of $1.0 M_{\odot}$. By

enforcing $e = 0.4$, the mass sum is brought into agreement with the expectation, while the residuals do not increase. In the coming few years, the inner orbit of this triple will become fully constrained, but monitoring of the outer pair A,C must continue. Both inner and outer pairs in this low-mass triple system have retrograde motion suggestive of mutually aligned orbits.

17005+0635. This bright A7V star HIP 83223, resolved interferometrically by the CHARA team in 1985.52 (McAlister et al. 1987), is designated as CHR 59. The latest orbit with $P = 26.49$ yr was published by Tokovinin et al. (2022). It assumed that the CHARA observations in the 1990s and the modern SOAR data cover two opposite ends of a near-circular orbit. However, the CHARA observations did not constrain the quadrant (it can be flipped), despite the substantial magnitude difference of 2.3 mag. The AO measure by Roberts & Mason (2018) in 2004.5, while inaccurate, clearly indicates that the companion was resolved always in the same quadrant, hence the orbital period is two times shorter than assumed previously. This drastically revised orbit with $P = 13.11 \pm 0.06$ yr fits the data better than the previous 26 yr orbit. It corresponds to a mass sum of $3.0 M_{\odot}$ with the Hipparcos parallax of 13.26 ± 0.47 mas. The Gaia DR3 parallax of 15.06 ± 0.21 mas, although formally more accurate, is likely biased by the fast motion near the periastron (in 2014.44) and gives an even smaller mass sum of $2.0 M_{\odot}$. Observations near and after the next periastron in 2027 will help to further constrain this orbit.

19164+1433. This early-type (HD 185055, B9V, $V = 5.63$ mag) pair was also resolved in 1985 by CHARA in their survey of bright stars (McAlister et al. 1987). The orbit with $P = 13.67$ yr was published by Tokovinin et al. (2015). Here it is revised drastically to $P = 6.9$ yr. The quadrants of the SOAR measures are known, showing that the pair is always resolved in the same quadrant, and the orbit is eccentric. The situation resembles the previous case, but here observations near the periastron are actually available, confirming the eccentric orbit. Gaia DR3 measured an accurate parallax of 6.244 ± 0.034 mas for the tertiary companion B located at $8''.3$, while the astrometry of the inner binary is biased by the fast orbital motion. With this parallax, the new orbit corresponds to the mass sum of $5.2 M_{\odot}$.

4.3. Spurious Visual Pairs: HD 129732

The star HD 129732 (A1IV, $V = 7.37$ mag) was presumably resolved at $0''.4$ by R. Innes in 1909 and it was designated as I 528. The WDS database contains two more visual resolutions in 1927 and 1930 at much closer separations of $0''.1$ and several visual non-resolutions. In

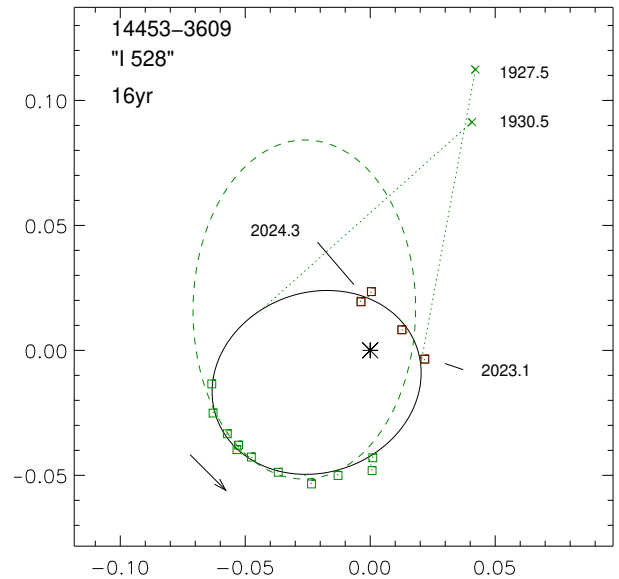


Figure 5. Orbits of 14453–3609 with periods of 15.9 yr (full line) and 31.8 yr (dash). Two discrepant visual measures are plotted by crosses and connected to the ephemeris positions by dotted lines.

the modern epoch, the pair remained unresolved by Hipparcos and was twice (in 1989 and 1993) resolved by the CHARA team. The HRCam measures cover the 2008–2024 interval (in 2008.5 the pair was unresolved). An orbit with $P = 33$ yr was fitted to the measures in 2018 and slightly refined by Tokovinin et al. (2022). In the light of recent observations near the periastron (Figure 5), this orbit appears to be incorrect, and the actual period is 15.93 ± 0.16 yr. All three visual measures turn out to be spurious; in fact, this pair *never* has been resolved visually. An attempt to match the two misleading visual measures is one of the reasons for computing the previous (wrong) orbit.

Speckle observations reveal many cases of spurious visual resolutions, sometimes “confirmed” by several subsequent measures. Lists of such spurious pairs are published regularly (e.g. Mason et al. 2023). Here, the star in question is indeed binary, but its visual resolutions are nevertheless spurious. Another example is HIP 104440 (HD 200525, I 379, WDS 210094–7310), presumably discovered by Innes at $1''$. It has an eccentric visual-spectroscopic orbit with a maximum separation of $0''.3$ (Tokovinin 2023). The ORB6 catalog even contains two *orbits of single stars* based on their multiple spurious visual measures! Both pairs, 104 Tau (WDS 05074+1839, A 3010) (Tokovinin 2012) and HD 21161 (WDS 03244–1539, A 2909) (Tokovinin 2019), were “discovered” by R. Aitken, one of the most experienced and trusted visual observer of the past.

4.4. Spurious Visual Pairs: HR 6100

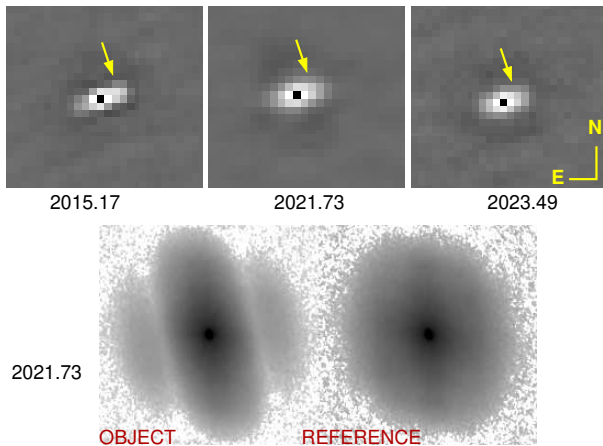


Figure 6. Top row: three shift-and-add images of HR 6100 suggesting resolutions in the same quadrant (black dots mark the center). The speckle power spectra of the object and the reference star taken in 2021.73 are shown below.

The bright ($V = 5.42$ mag, B8V) star HR 6100 (HD 147628, HIP 80390) belongs to the Upper Scorpius association with an age of 8–20 Myr. The Gaia DR3 parallax of 7.65 ± 0.12 mas is close to the DR2 parallax of 7.89 mas and to the Hipparcos parallax of 7.75 ± 0.25 mas. So, the binary nature of the source apparently did not spoil its astrometry.

In 1927, [van den Bos \(1928\)](#) resolved this star as a visual binary at a separation of $0''.11$, with nearly equal components. It has been measured in the period 1927–1947 three times by himself and twice by W. Finsen, apparently confirming this discovery. The pair is denoted as B 868 and 16245–3734. However, the WDS database also documents 13 non-resolutions (or partial resolutions) by visual observers between 1936 and 1968. The early speckle interferometry resolved the binary, with three measures in 1989 and 1991 at separations between 30 and 56 mas ([McAlister et al. 1990](#); [Hartkopf et al. 1993, 1996](#)). The pair was not resolved by Hipparcos, hence around 1991 it was closer than $0''.1$.

Starting from 2008, this bright and close binary was frequently visited by HRCam using the y filter (central wavelength 540 nm). The magnitude difference of ~ 0.5 mag allows identification of the correct quadrant from the shift-and-add (SAA) images at times of maximum separation. Figure 6 gives the three best examples indicating that in 2015.17, 2021.73, and 2023.49 the companion was located on the upper-right side, in the same quadrant. In 2015 the data were recorded with a 5 ms exposure time and the speckle contrast was higher than with the 25 ms exposures used later. At maximum separation, the second fringe in the power spectrum is clearly

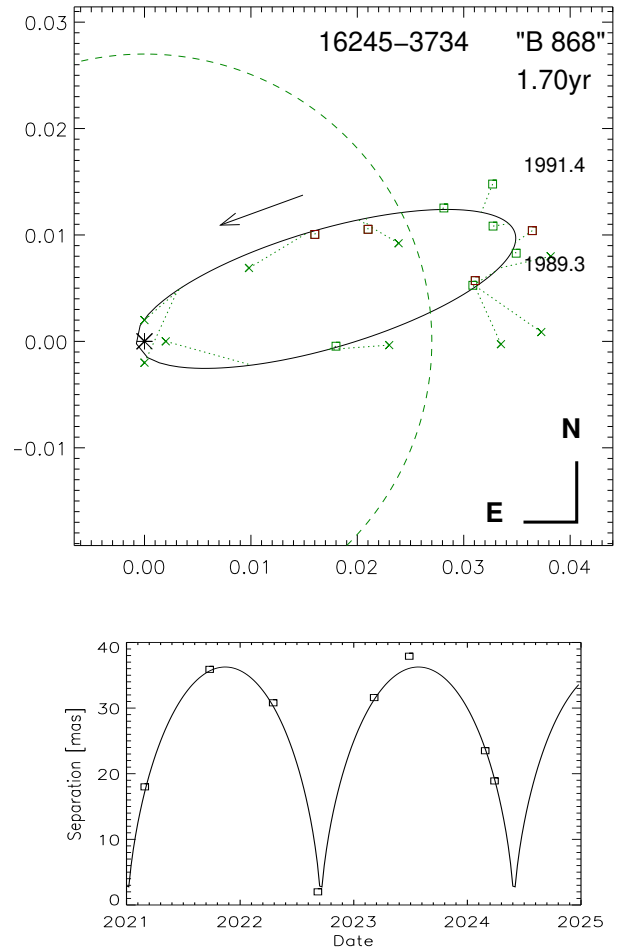


Figure 7. the orbit of HR 6100. Accurate positions are plotted as squares, less accurate as crosses (including three non-resolutions arbitrarily placed at 2 mas separation). The dashed circle indicates the diffraction limit of 27 mas. The lower plot shows separation vs. time.

detected, allowing very accurate position measurements (using a reference star), but at separations below the formal diffraction limit of 27 mas, only the central fringe is present. Measurements under the diffraction limit are less accurate, they are obtained by fixing Δm . Larger errors are also assigned to the HRCam measurements made without reference stars. In three visits, the pair was securely unresolved, indicating separations well below 10 mas.

The HRCam data allow calculation of an eccentric orbit with a period of 1.70 yr, shown in Figure 7. According to this orbit, the separation never exceeds 38 mas, just above the diffraction limit of 4 m telescopes. Three secure non-resolutions at SOAR correspond to the epochs near periastron. If some position angles are flipped, the data can be fitted by an orbit with a small eccentricity and two times longer period, but such or-

bit contradicts the known quadrants. The free fit converges to a face-on orbit with $i = 0$, so the inclination is fixed to a small but more probable value of 20° . The weighted residuals of 1.6 mas match the estimated measurement errors, but a substantial uncertainty in the elements a, Ω, ω, i remains because the periastron is not covered. The orbit gives a mass sum of $5.5 M_\odot$ (parallax 7.65 mas), close to the masses estimated from the absolute magnitudes. However, adopting a larger eccentricity leads to a larger mass sum, so the orbit does not yet provide useful constraints on the mass. Rather, it does not contradict the expected masses and distance. Accurate masses can be measured only by observing this pair near the periastron with long-baseline interferometers.

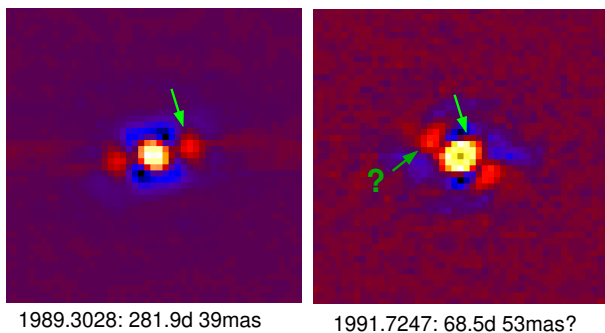


Figure 8. Speckle DVA images of HR 6100 from the CHARA archive (courtesy B. Mason). The green arrows mark the companion’s location according to the orbit. The darker green arrow with a question mark indicates the published position in 1991.72.

Of the three speckle measures published by CHARA, the first one in 1989.30 fits the orbit, the measure in 1991.39 is marked as uncertain and can be ignored, and the measure in 1991.72 ($68^\circ 5', 0'' 053$) is in strong disagreement; the orbit predicts $295^\circ 0', 0'' 029$. On my request, B. Mason reviewed these data. Figure 8 shows the Directed Vector Autocorrelation (DVA) images recorded by CHARA at two epochs. In both, the companion is separated by ~ 6 image pixels, but the published separations of 39 and 53 mas indicate a coarser pixel scale in 1991.72. On the 1991.72 DVA image, the central and side peaks are elongated in the direction predicted by the orbit. Apparently, the pair, separated by 29 mas according to the orbit, has not been resolved, while the measured peak at 59 mas is spurious. Similar spurious details, called optical ghosts, are also documented in the HRCam data (see Figure 11 in Tokovinin et al. 2010). They are distinguished from the real companions by observing reference stars and by comparison with observations of other stars made close in time.

The reported visual resolutions of HR 6100 appear to be spurious. With the 0.7 m telescopes used by the visual observers, the image elongation is always totally negligible. As noted above, this is not a unique case. Hypothetically, the eccentric orbit of this young pair could shrink through energy dissipation near periastron via tides or friction with the residual gas. If the semimajor axis has shortened substantially during ~ 100 yr, the visual resolutions could be explained. However, such a fast orbit decay implies the energy dissipation rate exceeding the luminosity of the stars by a large factor of ~ 30 , while in fact the luminosity is normal and matches the age, and the brightness is constant. Sharma et al. (2022) discovered only minor photometric pulsations of this object with frequencies of 2.54 and 2.59 cycle day^{-1} , typical of rapidly rotating ($V \sin i = 160 \text{ km s}^{-1}$) B-type stars.

4.5. Drastic Orbit Revisions

In this Subsection, examples of substantial orbit revisions are given (Figure 9). All orbits are based on the combination of visual and speckle measurements and have periods ranging from decades to centuries. The reasons of the revision are detailed below.

00024+1047. The pair A 1249AB (HIP 190) passed through the periastron in 2003 and is presently approaching the apastron. Almost two 59 yr orbital cycles are covered since its discovery by Aitken in 1905. The previous 129 yr quasi-circular orbit by Zirm (2003) flipped the speckle measures made by CHARA and all visual measures, although with the magnitude difference of $\Delta m = 0.8$ mag the flips of the visual measures are questionable. The tertiary companion C at $63''$ (HIP 185) has an accurate Gaia DR3 parallax of 10.08 ± 0.15 mas. The mass sum of A,B according to the new orbit, $2.26 M_\odot$, matches the spectral type G0 and the masses estimated from the luminosity better than the Zirm’s orbit, which yields a mass sum of $2.8 M_\odot$.

04123+0939. O. Struve resolved the F0 star HD 26547 at $0''.4$ in 1849 (Struve 1878). The pair has closed down and remained unresolved until 1894; its slow widening and closing at nearly constant angle is well documented by visual observations in the 20th century. The magnitude difference of $\Delta m = 1.2$ mag does not allow quadrant flips. The CHARA speckle observations cover the approach to the periastron in 1996, and presently the pair opens up again. So, the previous 272 yr orbit by Josties & Mason (2019) is not correct. No measurements of the parallax are available.

05005+0506. This G2/3V star HIP 23277 was resolved by O. Struve in 1847 at $0''.82$. It moves slowly on a slightly curved segment of its long-period orbit

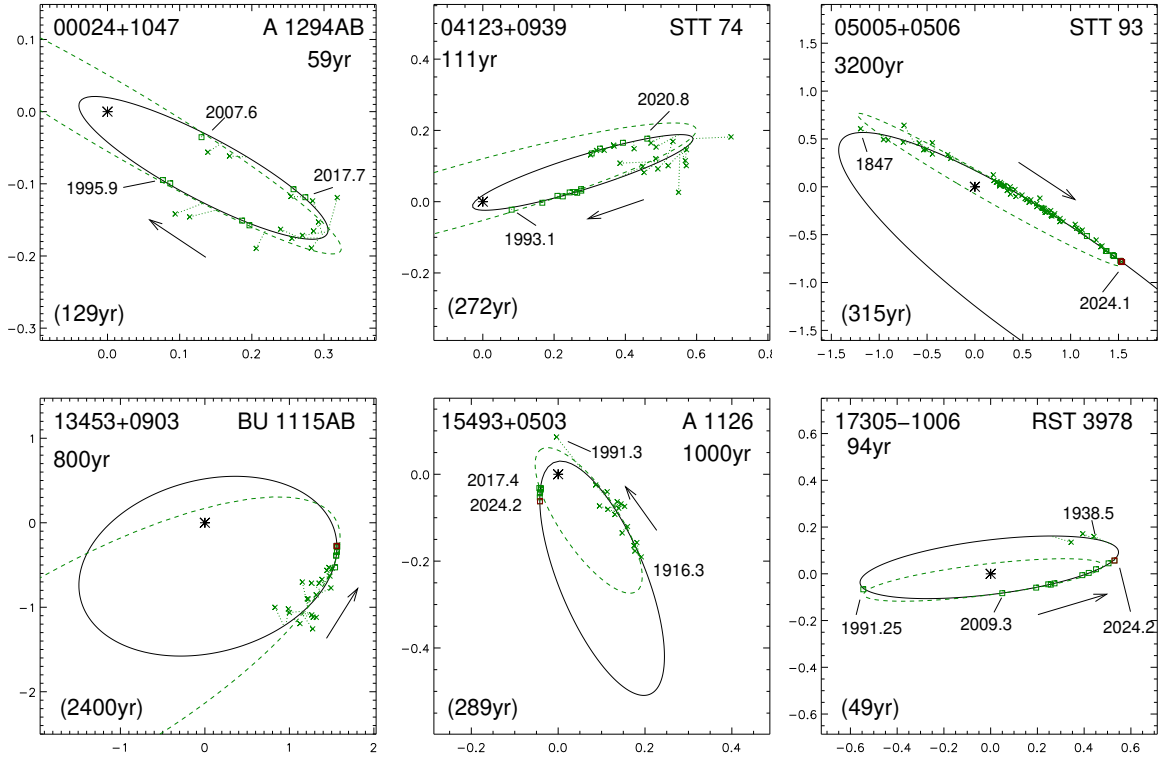


Figure 9. Six strongly revised orbits. All these pairs were discovered visually. Their WDS codes, discoverer designations, and revised periods are indicated, while periods of the previously computed orbits are given in brackets.

and presently is at $1''.73$ separation. Although the observed arc covers nearly 180° , it does not constrain the orbit, so I fixed the period and the eccentricity and fitted the remaining elements. Gaia DR3 measured both stars at a separation of $1''.278$, position angle $246^\circ.2$, $\Delta G = 0.606$ mag (in 2016.0) with matching parallaxes of 14.94 ± 0.03 mas and 15.02 ± 0.07 mas. The parallaxes and the new orbit correspond to the mass sum of $2.0 M_\odot$, in agreement with the spectral type. In contrast, the 315 yr orbit computed by [Izmailov \(2019\)](#) from essentially the same data yields an unrealistically large mass sum of $16.7 M_\odot$ and deviates from the latest accurate measurements. Although the new orbit is poorly constrained, it accurately models the observations and can be used for retroactive or near-term calibration of speckle measures.

13453+0903. This pair, HIP 67115 (G5, parallax 16.70 mas) resembles the previous one: only a short arc of its orbit is covered by the existing measures from 1873 to 2024. Here, the previous orbit computed by [Izmailov \(2019\)](#) is revised in the opposite sense, from the long 2400 yr to a shorter 800 yr period. The reason for this revision is the mass sum, reduced from 8.8 to $1.9 M_\odot$, and the systematic residuals of the accurate measures to the old orbit. Again, I fixed P and e and fitted the remaining elements. This orbit is also a good calibrator of

pixel scale and orientation tied to Gaia, which measured both components.

15493+0503. The pair HIP 77489 (K0, parallax 2.60 ± 0.04 mas) has a visual coverage from 1905 to 1966, and during this time the separation slowly decreased. One speckle measure by CHARA in 1991.32 is available, and the segment with increasing separation between 2017 to 2024 (after passage through the periastron) is well covered by seven HRCam measures. The small Δm allows quadrant flips. The 289 yr orbit by [Gómez et al. \(2022\)](#) substantially deviates from the recent measures, calling for its revision (see the dashed line in Figure 9). I could not reconcile the 1991.3 speckle measure with the latest observations and prefer to ignore it. The orbit is poorly constrained, so I fixed its period. The mass sums for the old and new orbits are 5.2 and $1.4 M_\odot$, respectively. The latter value matches the spectral type and the absolute magnitude of $M_V \approx 5.8$ mag, suggesting that the stars are not evolved.

17305-1006. HIP 85565 (G8V, parallax 19.96 ± 0.44 mas) was resolved by R. Rossiter in 1938 at $110^\circ.2$, $0''.47$ ([Rossiter 1955](#)). Only three visual measures were made by Rossiter, showing little motion till 1951. The magnitude difference of 2 mag should not allow quadrant flips. The Hipparcos and HRCam data together cover almost half of the orbit and indicate a period around 90

yr. Yet, the previously computed orbit (Tokovinin et al. 2015) had a period of 49 yr, postulating that the visual and Hipparcos positions are in the same quadrant and that the pair has made one revolution in-between. This orbit, however, yields an implausible mass sum of $11.7 M_{\odot}$. In the revision, I flipped the three visual measures instead of simply ignoring them and obtained a mass sum of $2.7 M_{\odot}$. The quadrant flip of the visual measures can possibly be justified by the human nature of the observer. If the first measure was attributed to the wrong quadrant by error, subsequent measures made by the same person were placed in the same quadrant in order to be consistent.

4.6. Tentative Orbits

The previous Section contained some poorly constrained long-period orbits based on short arcs. Here, another flavor of first-time tentative orbits based on scarce data is illustrated by three examples (Figure 10).

05251–3803. The 250 yr orbit of HD 35724 based on only five positions (three visual and two speckle) represents an extreme case. The discovery measure by Innes in 1927 is ignored because of the largely discrepant separation, and the remaining three visual measures in 1932–1937 do not show any significant motion. The two HRCam measures in 2018 and 2024 indicate that the motion is direct. These clearly insufficient data match an orbit with $P = 250$ yr. By fixing also the eccentricity $e = 0.7$, I obtain a converging LS fit and a mass sum of $3.0 M_{\odot}$ (parallax 4.17 ± 0.32 mas, spectral type F3V). This “guesstimate” orbit predicts that by 2031 the pair will turn by 10° and will close down to $0''.12$, accelerating toward the periastron in 2045.

10407–0211. The visual pair HD 92484 (G5) was resolved in 1906 at $0''.45$ by R. Aitken. A preliminary orbit with $P = 169$ yr is proposed here. The visual measures until 1983, when the pair became too close, show a retrograde motion. The two HRCam measures after passage through the periastron in 1991 are attributed to the second quadrant (with $\Delta m \approx 0.15$ mag, the quadrant is uncertain). An alternative orbit with a longer period is possible if the HRCam measures are flipped. As the orbit segment near the periastron is not covered, I fixed $e = 0.9$ in the LS fit.

Gaia DR3 contains two sources at $0''.4073$ separation with $\Delta G = -0.006$ mag; neither of them has 5-parameter astrometry. The separation is close to the orbit prediction, while the position angle is clearly discrepant. The orbit predicts $48^{\circ}58$ in 2016.0, while Gaia measured $79^{\circ}66$. A likely reason of the Gaia error is misidentification between the two sources in different scans. The resulting discrepant abscissae do not yield

acceptable 5-parameter astrometric models. Indirectly, this suggestion is supported by the near-zero magnitude difference: if the sources are swapped frequently, their mean fluxes will be nearly the same. Source swapping is mentioned by Holl et al. (2023), who discuss various caveats of the Gaia data related to non-point sources. The comparison of the HRCam calibrator binaries with Gaia DR3 (Tokovinin et al. 2022) revealed several discrepant pairs; in all of those, one or both components lacked the full 5-parameter astrometric solutions in DR3, indicating problematic Gaia astrometry.

14056–3916. HIP 68831 (G3V, parallax 6.82 ± 0.15 mas) was resolved for the first time at $0''.22$ in 1927 by Innes. The pair was apparently unresolved visually after 1934, re-appearing again in 1960 (I ignored this discrepant measure) and measured twice in 1979 and 1985. The quadrant of the Hipparcos measure agrees with these visual resolutions; no measures were made by CHARA. The three HRCam points show increasing separation after the periastron passage in 2018. Overall, the orbit looks as almost constrained (I fixed only the inclination) and leads to the mass sum of $1.9 M_{\odot}$.

5. DISCUSSION, RECOMMENDATIONS, AND TRENDS

In this work, the challenge of the visual orbit calculation is illustrated by examples ranging from trivial minor adjustments to radical revisions and tentative poorly constrained orbits. In all cases, understanding the nature and reliability of the input data is crucial. The system of relative weights and grades adopted in ORB6 (Hartkopf et al. 2001) is rooted in the epoch of visual measures and nowadays becomes obsolete. Excessive weight ascribed to the visual data (compared to speckle) degraded the quality of orbits published in Tokovinin et al. (2015), so many of these orbits had to be revised later to bring them into agreement with the accurate modern measures (two such examples are found in Table 1). A large effort of orbit calculation undertaken by Izmailov (2019) was also based on the formal fitting without prior manual data inspection and without a sanity check of the mass sum; consequently, some of those orbits also require substantial revisions (Figure 9).

The database of historic visual double star measures is an amazing heritage, allowing us to determine orbits with periods measured in centuries. However, the existing visual data cover only relatively bright pairs. Whenever their quality and quantity was adequate, the orbits were already computed, and only their improvement is possible by continued speckle monitoring. The remaining visual pairs without orbits typically have insufficient

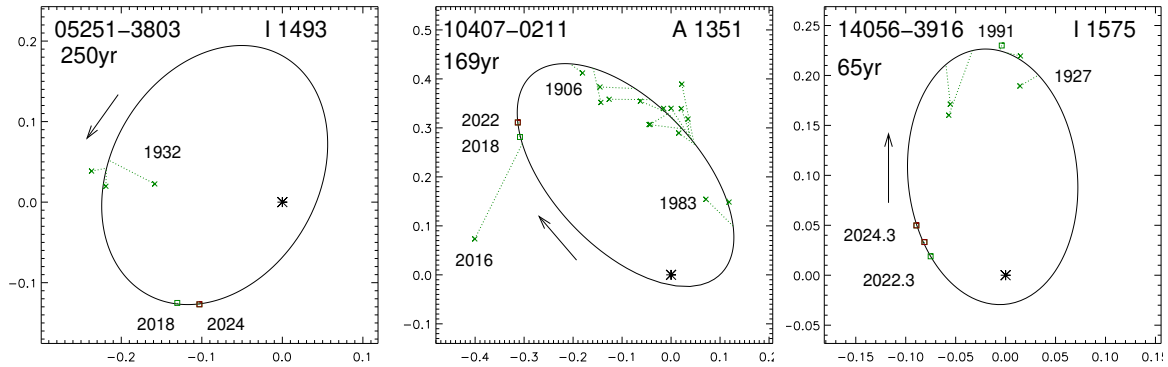


Figure 10. Three poorly constrained orbits.

historic data, and even when they are complemented by several modern observations, the resulting orbits are poorly constrained (e.g. 14407–0211 in Figure 10). So, the treasure trove of the old observations is not very deep and eventually it will be exhausted. We are indebted to R. Gould who explored the WDS content in search of pairs where modern observations could lead to an orbit. This effort in double star archaeology, in combination with the HRCam data, has led to many new orbits, although some of those are tentative owing to the scarce data.

My experience in computing orbits based on visual and speckle measures is summarized in the following recommendations.

- When the accurate (speckle or other) data are available, the old visual measures should not be used. Effectively, they add noise and degrade the quality of the orbit, instead of improving it.
- Historic visual measures should be used with caution. The separations are often strongly biased. The number of wrong resolutions (when the pair was in fact too close or the star is single) is substantial, as well as the number of discrepant measures. Manual inspection and editing (selective rejection or down-weighting) of visual data is mandatory in all cases. When both visual and speckle measures are used, they must be weighted according to their real errors.
- Not all speckle data are correct, their rejection is acceptable. There are some spurious speckle resolutions.
- The accuracy of the speckle data depends not only on the aperture size of the telescope, but also on the magnitude difference, magnitude, used equipment, measurement method, and the team that produced the data.

- For pairs closer than $\sim 2''$, relative positions provided by Gaia can be incorrect, possibly owing to confusion between the two sources. Existence of the 5-parameter astrometric solutions for both components of a pair is necessary for trusting the relative positions in DR3.

The classical epoch, when an implicit goal was to compute an orbit of every pair with observed motion, is coming to an end. Below I outline the future trends in the orbit calculation.

The Hipparcos mission discovered thousands of close pairs missed by the visual surveys. A rapid orbital motion was expected and confirmed for close Hipparcos binaries in the solar neighborhood, and the follow-up speckle effort produced their orbits (e.g. Horch et al. 2015). Similarly, fast movers among recently resolved nearby stars (mostly low-mass dwarfs), when regularly monitored, allow determination of good-quality orbits (Mann et al. 2019; Vrijmoet et al. 2022). In all these cases, we do not have to deal with the historic visual data, but a good understanding of the nature of Hipparcos and speckle measures is still needed for computing orbits.

Extrapolating the Hipparcos results to Gaia opens new exciting horizons. The number of astrometric orbits in DR3, $\sim 10^5$, already largely exceeds the content of ORB6 (Halbwachs et al. 2023). However, those orbits have only short periods (less than ~ 3 years), and a substantial fraction of low-quality solutions. The median period of solar-type binaries is of the order of 10^5 days or 300 yr (Raghavan et al. 2010), while the planned duration of the Gaia mission is only 10 yr. So, even the final Gaia data release (DR5) will determine astrometric orbits for a minor fraction of nearby binaries, and the orbit catalogs like ORB6 will remain relevant for slower pairs. Furthermore, a direct resolution of astrometric binaries is needed to derive masses even when their Gaia orbits are known (the mass sum depends on the full semimajor axis, while Gaia measures only the axis of

the photocenter). Another essential ingredient are accurate parallaxes. For visual binaries, Gaia either does not provide parallaxes or gives distorted values because the standard 5-parameter astrometric solutions are biased by the orbital motion (Chulkov & Malkov 2022). This bias is removed for binaries with astrometric orbits and partially corrected for acceleration solutions. However, when the individual transits become public in DR4 (expected in 2026), their joint analysis together with relative positions and visual orbits will de-bias the parallaxes and lead to accurate masses. So, the continuation and extension of the ground-based speckle interferometric monitoring appears to be an essential complement to Gaia.

The Gaia mission will eventually publish millions of new faint pairs with separations above $\sim 0''.1$ in the final DR5; at the same time, the quality and quantity of Gaia astrometric orbits will improve, compared to the current DR3. The overwhelming majority of new Gaia binaries will be distant and will move too slowly. So, the future effort of monitoring and orbit calculation must be selective, as was the case with the Hipparcos pairs. The estimated periods P^* and the periods of astrometric orbits will serve for selecting a subset of fast movers among Gaia binaries. Instead of aiming to compute orbits of all pairs with detectable motion, future follow-up observations using speckle interferometry and other methods will be motivated by the use of these orbits. For the measurements of masses, for example, only a subset of fast movers will be sufficient, while the requisite high accuracy of position measurements favors long-baseline interferometers rather than speckle interferometry, especially for massive and bright stars. The new pairs discovered by Hipparcos, Gaia, and high-resolution imaging surveys lack historic measures, so the time coverage

will be a critical consideration for calculation of their orbits. Orbits of long-period binaries of interest (e.g. exohosts or PMS stars) will be estimated approximately from short observed arcs.

A shift of the paradigm from holistic to selective observations means that the orbital motion of the majority of binaries (both historic and new) will no longer be monitored. If, in the future, some of those systems become interesting, they will lack the time coverage for orbit calculation. This is particularly sensitive for orbits with large eccentricity. If we want to preserve the holistic strategy, monitoring a large number of pairs will require a dedicated facility, e.g. a pair of 2 m robotic telescopes in both hemispheres equipped with speckle imagers.

I thank B. Mason for extracting historic data from the WDS database and for examination of the CHARA data on B 868. Comments by R. Matson on the paper draft are appreciated. This work used data from the Washington Double Star Catalog maintained at USNO and observations made at SOAR. This work used the SIMBAD service operated by Centre des Données Stellaires (Strasbourg, France), bibliographic references from the Astrophysics Data System maintained by SAO/NASA. This work has made use of data from the European Space Agency (ESA) mission Gaia (<https://www.cosmos.esa.int/gaia>) processed by the Gaia Data Processing and Analysis Consortium (DPAC, <https://www.cosmos.esa.int/web/gaia/dpac/consortium>). Funding for the DPAC has been provided by national institutions, in particular the institutions participating in the Gaia Multilateral Agreement.

Facility: SOAR

REFERENCES

- Aitken, R. G. 1935, *The binary stars* (New York and London, McGraw-Hill book company, inc.)
- Andersen, J. 1991, *A&A Rv*, 3, 91, doi: [10.1007/BF00873538](https://doi.org/10.1007/BF00873538)
- Blunt, S., Wang, J. J., Angelo, I., et al. 2020, *AJ*, 159, 89, doi: [10.3847/1538-3881/ab6663](https://doi.org/10.3847/1538-3881/ab6663)
- Borkovits, T., Hajdu, T., Sztakovics, J., et al. 2016, *MNRAS*, 455, 4136, doi: [10.1093/mnras/stv2530](https://doi.org/10.1093/mnras/stv2530)
- Brandt, T. D., Dupuy, T. J., Li, Y., et al. 2021, *AJ*, 162, 186, doi: [10.3847/1538-3881/ac042e](https://doi.org/10.3847/1538-3881/ac042e)
- Chulkov, D., & Malkov, O. 2022, *MNRAS*, 517, 2925, doi: [10.1093/mnras/stac2827](https://doi.org/10.1093/mnras/stac2827)
- Couteau, P. 1978, *L'observation des etoiles doubles visuelles, suivie d'un catalogue de 744 etoiles doubles pour tous instruments* (Paris: Flammarion)
- Docobo, J. A., & Costa, J. M. 1990, *IAU Commission 26 Information Circular*, 112, 1
- Evans, N. R., Schaefer, G., Gallenne, A., et al. 2024, arXiv e-prints, arXiv:2407.09641, doi: [10.48550/arXiv.2407.09641](https://doi.org/10.48550/arXiv.2407.09641)
- Finsen, W. S. 1936, *MNRAS*, 96, 862, doi: [10.1093/mnras/96.9.862](https://doi.org/10.1093/mnras/96.9.862)
- Gaia Collaboration, Brown, A. G. A., Vallenari, A., et al. 2021, *A&A*, 649, A1, doi: [10.1051/0004-6361/202039657](https://doi.org/10.1051/0004-6361/202039657)
- Gómez, J., Docobo, J. A., Campo, P. P., et al. 2022, *MNRAS*, 509, 4229, doi: [10.1093/mnras/stab2633](https://doi.org/10.1093/mnras/stab2633)

- Halbwachs, J.-L., Pourbaix, D., Arenou, F., et al. 2023, *A&A*, 674, A9, doi: [10.1051/0004-6361/202243969](https://doi.org/10.1051/0004-6361/202243969)
- Hartkopf, W. I., Mason, B. D., Barry, D. J., et al. 1993, *AJ*, 106, 352, doi: [10.1086/116644](https://doi.org/10.1086/116644)
- Hartkopf, W. I., Mason, B. D., McAlister, H. A., et al. 1996, *AJ*, 111, 936, doi: [10.1086/117841](https://doi.org/10.1086/117841)
- Hartkopf, W. I., Mason, B. D., & Worley, C. E. 2001, *AJ*, 122, 3472, doi: [10.1086/323921](https://doi.org/10.1086/323921)
- Hartkopf, W. I., McAlister, H. A., & Franz, O. G. 1989, *AJ*, 98, 1014, doi: [10.1086/115193](https://doi.org/10.1086/115193)
- Heintz, W. D. 1978, *Double stars*, Vol. 15 (Geophysics and Astrophysics Monographs, Dordrecht: Reidel)
- Holl, B., Fabricius, C., Portell, J., et al. 2023, *A&A*, 674, A25, doi: [10.1051/0004-6361/202245353](https://doi.org/10.1051/0004-6361/202245353)
- Horch, E. P., van Belle, G. T., Davidson, James W., J., et al. 2015, *AJ*, 150, 151, doi: [10.1088/0004-6256/150/5/151](https://doi.org/10.1088/0004-6256/150/5/151)
- Hwang, H.-C., Ting, Y.-S., & Zakamska, N. L. 2022, *MNRAS*, 512, 3383, doi: [10.1093/mnras/stac675](https://doi.org/10.1093/mnras/stac675)
- Izmailov, I. S. 2019, *Astronomy Letters*, 45, 30, doi: [10.1134/S106377371901002X](https://doi.org/10.1134/S106377371901002X)
- Josties, J., & Mason, B. D. 2019, *IAU Commission 26 Information Circular*, 199, 1
- Klement, R., Rivinius, T., Gies, D. R., et al. 2024, *ApJ*, 962, 70, doi: [10.3847/1538-4357/ad13ec](https://doi.org/10.3847/1538-4357/ad13ec)
- Lester, K. V., Howell, S. B., Matson, R. A., et al. 2023, *AJ*, 166, 166, doi: [10.3847/1538-3881/acf563](https://doi.org/10.3847/1538-3881/acf563)
- Lucy, L. B. 2014, *A&A*, 563, A126, doi: [10.1051/0004-6361/201322649](https://doi.org/10.1051/0004-6361/201322649)
- . 2018, *A&A*, 618, A100, doi: [10.1051/0004-6361/201732145](https://doi.org/10.1051/0004-6361/201732145)
- Mann, A. W., Dupuy, T., Kraus, A. L., et al. 2019, *ApJ*, 871, 63, doi: [10.3847/1538-4357/aaf3bc](https://doi.org/10.3847/1538-4357/aaf3bc)
- Mason, B. D., Tokovinin, A., Mendez, R. A., & Costa, E. 2023, *AJ*, 166, 139, doi: [10.3847/1538-3881/acedaf](https://doi.org/10.3847/1538-3881/acedaf)
- Mason, B. D., Wycoff, G. L., Hartkopf, W. I., Douglass, G. G., & Worley, C. E. 2001, *AJ*, 122, 3466, doi: [10.1086/323920](https://doi.org/10.1086/323920)
- McAlister, H., Hartkopf, W. I., & Franz, O. G. 1990, *AJ*, 99, 965, doi: [10.1086/115387](https://doi.org/10.1086/115387)
- McAlister, H. A., Hartkopf, W. I., Hutter, D. J., Shara, M. M., & Franz, O. G. 1987, *AJ*, 93, 183, doi: [10.1086/114297](https://doi.org/10.1086/114297)
- Offner, S. S. R., Moe, M., Kratter, K. M., et al. 2023, in *Astronomical Society of the Pacific Conference Series*, Vol. 534, *Protostars and Planets VII*, ed. S. Inutsuka, Y. Aikawa, T. Muto, K. Tomida, & M. Tamura, 275, doi: [10.48550/arXiv.2203.10066](https://doi.org/10.48550/arXiv.2203.10066)
- Pourbaix, D. 2000, *A&AS*, 145, 215, doi: [10.1051/aas:2000237](https://doi.org/10.1051/aas:2000237)
- Press, W. H., Flannery, B. P., & Teukolsky, S. A. 1986, *Numerical recipes. The art of scientific computing* (Cambridge: University Press)
- Raghavan, D., McAlister, H. A., Henry, T. J., et al. 2010, *ApJS*, 190, 1, doi: [10.1088/0067-0049/190/1/1](https://doi.org/10.1088/0067-0049/190/1/1)
- Rickman, E. L., Ceva, W., Matthews, E. C., et al. 2024, *A&A*, 684, A88, doi: [10.1051/0004-6361/202347906](https://doi.org/10.1051/0004-6361/202347906)
- Rizzuto, A. C., Dupuy, T. J., Ireland, M. J., & Kraus, A. L. 2020, *ApJ*, 889, 175, doi: [10.3847/1538-4357/ab5aed](https://doi.org/10.3847/1538-4357/ab5aed)
- Roberts, L. C., & Mason, B. D. 2018, *MNRAS*, 473, 4497, doi: [10.1093/mnras/stx2559](https://doi.org/10.1093/mnras/stx2559)
- Rossiter, R. A. 1955, *Publications of Michigan Observatory*, 11, 1
- Schaefer, G. H., Hummel, C. A., Gies, D. R., et al. 2016, *AJ*, 152, 213, doi: [10.3847/0004-6256/152/6/213](https://doi.org/10.3847/0004-6256/152/6/213)
- Sharma, A. N., Bedding, T. R., Saio, H., & White, T. R. 2022, *MNRAS*, 515, 828, doi: [10.1093/mnras/stac1816](https://doi.org/10.1093/mnras/stac1816)
- Stojanovski, Z., & Savransky, D. 2024, *AJ*, 168, 40, doi: [10.3847/1538-3881/ad4a5e](https://doi.org/10.3847/1538-3881/ad4a5e)
- Struve, O. 1878, *Pulkova Observations*, 9, 1
- Tokovinin, A. 2012, *AJ*, 144, 56, doi: [10.1088/0004-6256/144/2/56](https://doi.org/10.1088/0004-6256/144/2/56)
- . 2016, *ORBIT: IDL software for visual, spectroscopic, and combined orbits*, 1.0, Zenodo, doi: [10.5281/zenodo.61119](https://doi.org/10.5281/zenodo.61119)
- . 2017, *ApJ*, 844, 103, doi: [10.3847/1538-4357/aa7746](https://doi.org/10.3847/1538-4357/aa7746)
- . 2018a, *PASP*, 130, 035002, doi: [10.1088/1538-3873/aaa7d9](https://doi.org/10.1088/1538-3873/aaa7d9)
- . 2018b, *ApJS*, 235, 6, doi: [10.3847/1538-4365/aaa1a5](https://doi.org/10.3847/1538-4365/aaa1a5)
- . 2019, *Journal of Double Star Observations*, 15, 583
- . 2021a, *AJ*, 161, 144, doi: [10.3847/1538-3881/abda42](https://doi.org/10.3847/1538-3881/abda42)
- . 2021b, *Universe*, 7, 352, doi: [10.3390/universe7090352](https://doi.org/10.3390/universe7090352)
- . 2022, *AJ*, 163, 161, doi: [10.3847/1538-3881/ac5330](https://doi.org/10.3847/1538-3881/ac5330)
- . 2023, *AJ*, 165, 160, doi: [10.3847/1538-3881/acbe42](https://doi.org/10.3847/1538-3881/acbe42)
- Tokovinin, A., & Kiyaveva, O. 2016, *MNRAS*, 456, 2070, doi: [10.1093/mnras/stv2825](https://doi.org/10.1093/mnras/stv2825)
- Tokovinin, A., Mason, B. D., & Hartkopf, W. I. 2010, *AJ*, 139, 743, doi: [10.1088/0004-6256/139/2/743](https://doi.org/10.1088/0004-6256/139/2/743)
- Tokovinin, A., Mason, B. D., Hartkopf, W. I., Mendez, R. A., & Horch, E. P. 2015, *AJ*, 150, 50, doi: [10.1088/0004-6256/150/2/50](https://doi.org/10.1088/0004-6256/150/2/50)
- Tokovinin, A., Mason, B. D., Mendez, R. A., & Costa, E. 2022, *AJ*, 164, 58, doi: [10.3847/1538-3881/ac78e7](https://doi.org/10.3847/1538-3881/ac78e7)
- . 2024, *AJ*, 168, 28, doi: [10.3847/1538-3881/ad4d56](https://doi.org/10.3847/1538-3881/ad4d56)
- Tokovinin, A. A. 1983, *Soviet Astronomy Letters*, 9, 327
- Torres, G., Schaefer, G. H., Monnier, J. D., et al. 2022, *ApJ*, 941, 8, doi: [10.3847/1538-4357/ac9d8d](https://doi.org/10.3847/1538-4357/ac9d8d)
- van den Bos, W. H. 1928, *Annalen van de Sterrewacht te Leiden*, 14, D1
- . 1962, *PASP*, 74, 297, doi: [10.1086/127812](https://doi.org/10.1086/127812)

Vrijmoet, E. H., Tokovinin, A., Henry, T. J., et al. 2022,
AJ, 163, 178, doi: [10.3847/1538-3881/ac52f6](https://doi.org/10.3847/1538-3881/ac52f6)

Weis, E. W. 1974, ApJ, 190, 331, doi: [10.1086/152881](https://doi.org/10.1086/152881)

Zirm, H. 2003, IAU Commission 26 Information Circular,
151, 1

Zúñiga-Fernández, S., Olofsson, J., Bayo, A., et al. 2021,
A&A, 655, A15, doi: [10.1051/0004-6361/202141985](https://doi.org/10.1051/0004-6361/202141985)